

Supplementary Information

The emergence of a robust lithium gallium oxide surface layer on gallium-doped LiNiO₂ cathodes enables extended cycling stability

Mritunjay Mishra^b, Koffi P.C. Yao^{a*}

^a*Department of Mechanical Engineering, University of Delaware, Newark, Delaware 19716, United States of America.*

^b*Department of Chemistry and Biochemistry, University of Delaware, Newark, Delaware 19716, United States of America.*

Corresponding author email: claver@udel.edu

Literature survey of doped LiNiO₂ cycling

Table S1. Data table used for obtaining Fig.1 in the manuscript.

S.No.	Cathodes	% retention Cycle No.	Discharge Capacity (mAh·g ⁻¹)	C-rate/Current density	Ref.
1	LiNiO ₂	83 50	247.5		
	1%W-LiNiO ₂	95 50	242.7	C/10	
	1.5%W-LiNiO ₂	96 50	236.1	1C = 180 mA·g ⁻¹	1
	2%W-LiNiO ₂	97 50	225.9		
2	LiNiO ₂	79 50	216	C/10	
	0.2%Cu-LiNiO ₂	90 50	218	1C = 200 mA·g ⁻¹	2
3	LiNiO ₂	85 50	250	C/10	
	1.4%Zr-LiNiO ₂	95 50	232.6	1C = 180 mA·g ⁻¹	3
4	LiNiO ₂	57 50	203.76		
	1%Nb-LiNiO ₂	81 50	203.27	C/10	
	1.5%Nb-LiNiO ₂	85 50	221.20	1C = -	4
	2%Nb-LiNiO ₂	70 50	201.50		
5	LiNiO ₂	85 50	247.5	C/10	
	0.5% Zr-LiNiO ₂	92 50	246.5	1C = 180 mA·g ⁻¹	5
6	LiNiO ₂	88 50	232.97	C/10	
	Mg-LiNiO ₂	89 50	235.45	1C = 180 mA·g ⁻¹	6
	MgCu-LiNiO ₂	91 50	229.49		
7	LiNiO ₂	71 50	215.9	C/10	
	1%Nb-LiNiO ₂	92 50	188.1	1C = 270 mA·g ⁻¹	7
8	LiNiO ₂	77 50	161.8		
	LiNi _{0.975} Ga _{0.025} O ₂	45 50	174.4		
	LiNi _{0.975} Al _{0.025} O ₂	46 50	170.5	C/10	
	LiNi _{0.995} Ti _{0.005} O ₂	41 50	172.9	1C = -	8
	LiNi _{0.990} Al _{0.005} Ti _{0.005} O ₂	47 50	196.3		
9	LiNiO ₂	20 50	200	C/10	
	ZrO ₂ -LiNiO ₂	92 50	190	1C = 180 mA·g ⁻¹	9
10	LiNiO ₂	76 50	210.3	C/10	
	C ₄ H ₆ CoO ₄ -LiNiO ₂	87 50	214.7	1C = 180 mA·g ⁻¹	10
11	LiNiO ₂	51 50	210		
	2% Ga-LiNiO ₂	100 50	190	36 mA·g ⁻¹	11
	0.5% Ga-LiNiO ₂	83 50	180		
12	LiNiO ₂	57 50	230		
	1%Ga-LiNiO ₂	60 50	225		
	2%Ga-LiNiO ₂	80 50	225	C/10	
	3%Ga-LiNiO ₂	80 50	220	1C = 225 mA·g ⁻¹	
	4%Ga-LiNiO ₂	84 50	205		
	5%Ga-LiNiO ₂	83 50	190		
13	LiNiO ₂	88 50	209		
	2% Al-LiNiO ₂	89 50	221	C/10	
	4% Al-LiNiO ₂	88 50	185	1C = 200 mA·g ⁻¹	13
	6% Al-LiNiO ₂	85 50	181		
14	LiNiO ₂	52 50	240	C/10	14
15	LiNiO ₂	66 50	235.9		
	3%Al-LiNiO ₂	85 50	220.2	C/10	
	5%Al-LiNiO ₂	97 50	209.9	1C = 200 mA·g ⁻¹	15
16	LiNiO ₂	67 50	160	C/3	
	1%Al-LiNiO ₂	90 50	149	0.4 mA·cm ⁻²	16
	3%Al-LiNiO ₂	100 50	136		
17	0% Ga-LiNiO ₂	45 50	197	C/10	
	2% Ga-LiNiO ₂	50 50	192	1C = 180 mA·g ⁻¹	
	5% Ga-LiNiO ₂	84 50	174	This Work	

Table S2. Variance of the capacity retention value obtained from publications shown in Fig. 1 in introduction.

Dopants in LiNiO ₂	Variance (σ^2)	Standard deviation (σ)
Undoped	387	19.67
Gallium	283	16.82
Tungsten	5	2.24
Zirconium	76	8.72
Niobium	85	9.22
Aluminium	277	16.64

Energy Dispersive X-Ray Spectroscopy (EDS) measurements and analyses

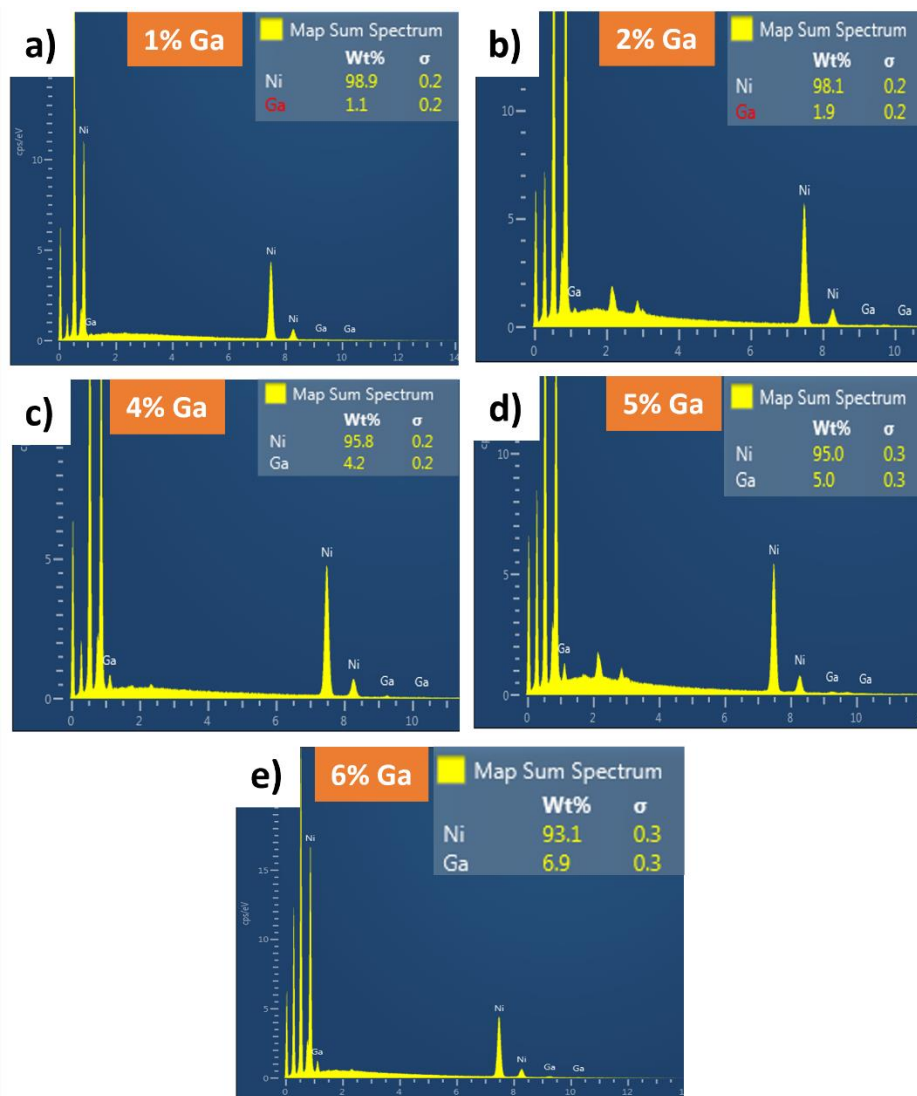


Fig. S1. (a-e) EDS spectrum of 0%-6% Ga-LiNiO₂ showing elemental composition obtained from one of the locations shown in Table S3.

Table S3. EDS data obtained from three distinct sites of 1% to 6% Ga-LiNiO₂.

S.No.	Compounds	Wt(%) from EDS Ga : Ni	Mole(%) from EDS Ga : Ni	Targeted Mole (%) Ga : Ni
1	1% Ga-LiNiO₂			
	Location 1	1.1 : 98.9	1.0 : 99.0	1 : 99
	Location 2	1.3 : 98.7	1.1 : 98.9	
	Location 3	1.4 : 98.6	1.2 : 98.8	
	Average		1.1 : 98.9	
2	2% Ga-LiNiO₂			
	Location 1	2.4 : 97.6	2.03 : 97.97	2 : 98
	Location 2	2 : 98	1.69 : 98.31	
	Location 3	1.9 : 98.1	1.61 : 98.39	
	Average		1.77 : 98.23	
3	4% Ga-LiNiO₂			
	Location 1	3.9 : 96.1	2.64 : 97.36	4 : 96
	Location 2	4.2 : 95.8	3.60 : 96.40	
	Location 3	5 : 95	4.24 : 95.76	
	Average		3.50 : 96.50	
4	5% Ga-LiNiO₂			
	Location 1	5.6 : 94.4	4.76 : 95.24	5 : 95
	Location 2	5 : 95	4.24 : 95.76	
	Location 3	5.7 : 94.3	4.84 : 95.16	
	Average		4.61 : 95.39	
5	6% Ga-LiNiO₂			
	Location 1	6.1 : 93.9	5.18 : 94.82	6 : 94
	Location 2	6.9 : 93.1	5.80 : 94.20	
	Location 3	7.1 : 92.9	6.04 : 93.96	
	Average		5.67 : 94.33	

X-ray Photoelectron Spectra (XPS) of 0%, 2%, and 5% Ga-LiNiO₂

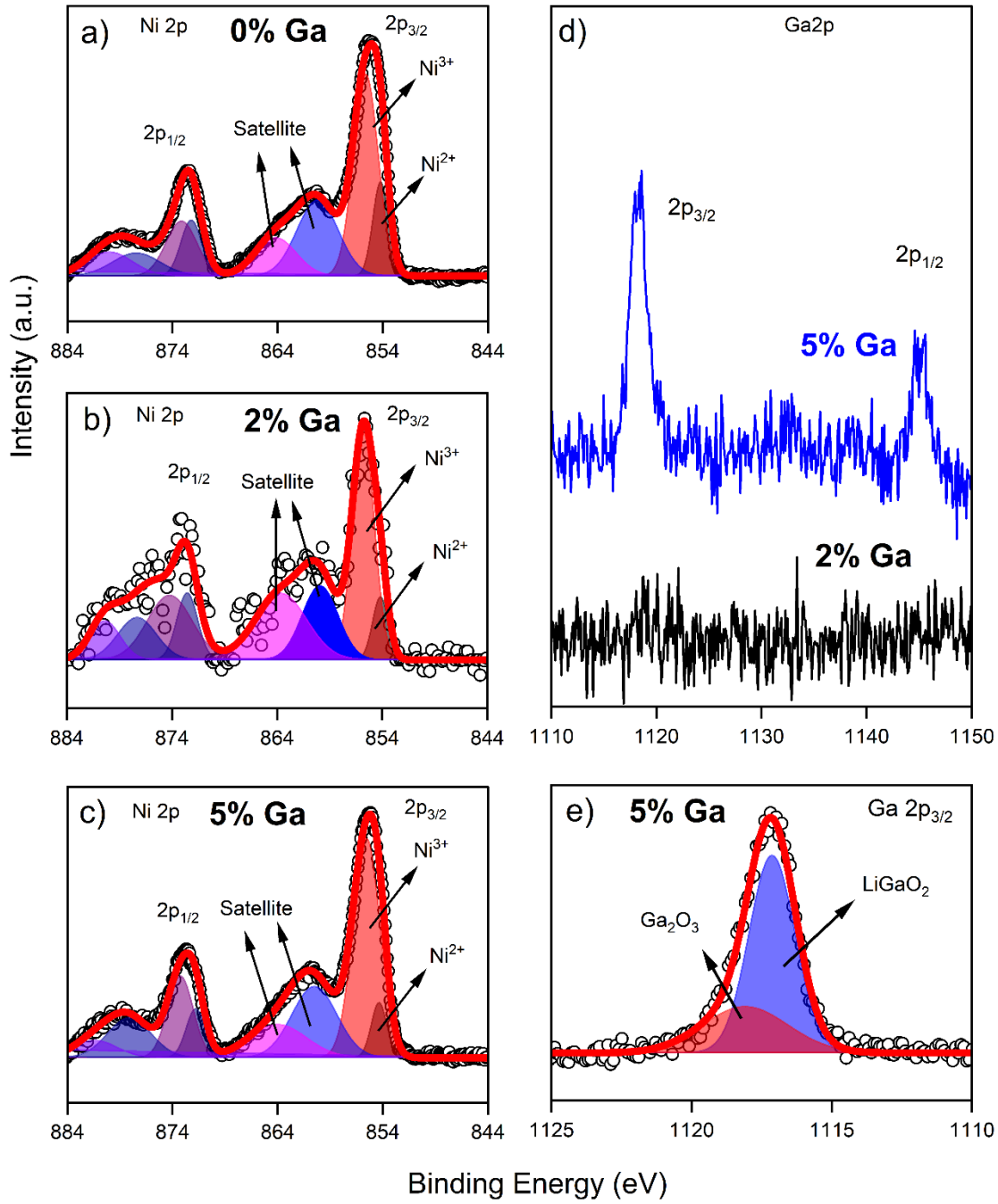


Fig. S2. Ni2p XPS of a) 0% Ga, b) 2% Ga, and c) 5% Ga-LiNiO₂. d) Ga2p XPS of 2% and 5%Ga-LiNiO₂. e) XPS spectra of Ga2p_{3/2} of 5% Ga-LiNiO₂.

XPS measurements were conducted on undoped and Ga-doped LiNiO₂ as shown in **Fig. S2a-c**. 2p orbital of Ni in 0%, 2%, and 5% Ga-LiNiO₂ yield a doublet (i.e., 2p_{3/2} and 2p_{1/2}) due to the spin-orbit coupling with the two possible states having different binding energies. Each energy state consists of Ni³⁺ and Ni²⁺ species along with their satellite peaks. The obtained XPS spectra were deconvoluted based on the previously reported XPS for nickel-rich oxide (NMC) cathodes.^{17,18} The deconvoluted XPS spectra

confirmed the presence of Ni³⁺ and Ni²⁺ in all three LiNiO₂ cathodes and their peak positions and area are tabulated in **Table S4**. In agreement with the observations of Wu et al.¹⁹ on LiNi_{0.8}Co_{0.1}Mn_{0.1-x}Ga_xO₂, a systematic increase in the Ni³⁺/Ni²⁺ ratio upon higher Ga doping is found, pointing to decreasing cation mixing.

The Ga 2p XPS spectra shown in **Fig. S2d** were acquired to characterize the surface phases present on 2% and 5% Ga doped LiNiO₂. No Ga signals were observed on the surface of 2% Ga due to bulk doping, however, intense Ga 2p peaks were seen for 5% Ga. To confirm the emergence of the LiGaO₂ phase on the surface of 5% Ga-LiNiO₂, XPS spectra were deconvoluted and shown in **Fig. S2e**. Deconvolution of the XPS spectra revealed two discernible peaks centered at 1117.13 eV and 1118.09 eV, respectively. The predominant peak observed at a lower binding energy of 1117.13 eV is attributed to the LiGaO₂ phase.²⁰ The minor peak appearing at a relatively higher binding energy of 1118.09 eV is associated with the Ga₂O₃ phase.^{20,21} This observation corroborates the dominance of the LiGaO₂ phase as a prominent constituent at the surface of the 5% Ga-LiNiO₂ material, as confirmed by the XRD, EDS and HRTEM analysis.

Table S4. Peak position and area ratio from XPS spectra deconvolution of 0%, 2%, and 5% Ga-LiNiO₂.

	Ni ²⁺		Ni ³⁺		Area Ratio (Ni ³⁺ /Ni ²⁺)
	Peak Position (eV)	Area (%)	Peak Position (eV)	Area (%)	
0% Ga-LiNiO ₂	854.20	22.80	855.61	77.20	3.38
2% Ga-LiNiO ₂	854.17	19.36	855.79	80.64	4.16
5% Ga-LiNiO ₂	854.35	12.57	855.54	87.43	6.95

X-ray diffraction (XRD) patterns of as-synthesized 0%, 1%, 2%, 4%, 5% and 6% Ga doped LiNiO₂

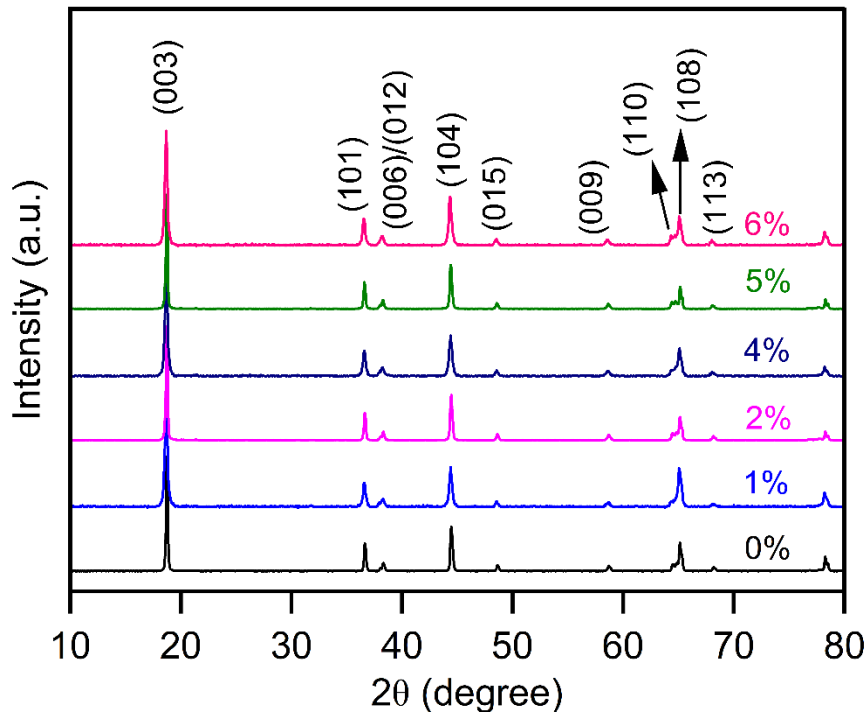


Fig. S3. XRD pattern of 0%-6% Ga-doped LiNiO₂ pristine powder electrodes.

Close inspection of the X-ray diffraction (XRD) patterns of as-synthesized undoped and Ga doped LiNiO₂

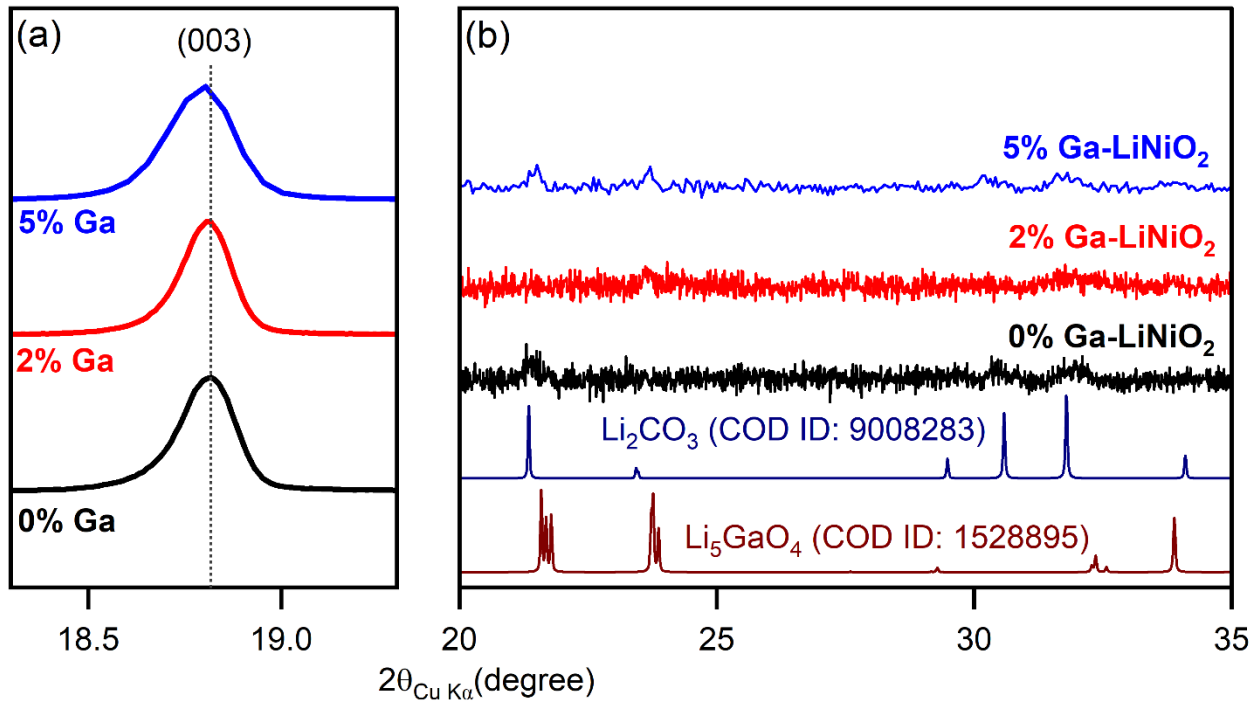


Fig. S4. (a) Magnified XRD at the (003) plane peak of 0%, 2%, and 5% Ga-LiNiO₂ showing shift and broadening of the plane with increasing Ga content. (b) Magnification of the 20°-35° range for comparison against Li_2CO_3 and Li_5GaO_4 reference PDFs .

Table S5. 2θ and FWHM value of (003) reflection corresponding to 0%, 2%, and 5% Gallium doped LiNiO₂.

	2θ of (003)	FWHM
0% Ga-LiNiO ₂	18.8060 ± 0.0016	0.16844 ± 0.00383
2% Ga-LiNiO ₂	18.8027 ± 0.0016	0.15270 ± 0.00359
5% Ga-LiNiO ₂	18.7888 ± 0.0043	0.20316 ± 0.01041

Rietveld refinement analysis of 0%, 2% and 5% Ga-doped LiNiO₂

In the structural model, we performed refinement on several key parameters, including the unit cell parameters, site occupancy, oxygen z-coordinate, and the isotropy U_{iso} parameters for oxygen (O), lithium (Li), gallium (Ga), and nickel (Ni) atoms. The following constraints were used:

- Similar U_{iso} parameters for atoms occupying the same Wycoff site.
- The total occupancy of the 3a and 3b sites in a given R̄3m phase adds to 1.
- The Ga content must be reasonably near the values targeted and measured by Energy dispersive X-ray spectroscopy (EDS).

It should be noted that Ga was investigated at several sites (i.e., 3a, 3a+3b, and 3b) and the best convergence was selected. At convergence, Ga appears to prefer the 3a sites within LiNiO₂. Similar observations were made by Kitsche et al.¹² The possibility of Ga occupying Ni site has not been excluded, however.

Crystallographic coordinates corresponding to Wycoff sites are as follows:

3a: (0, 0, 0), (1/3, 2/3, 2/3), (2/3, 1/3, 1/3)

3b: (0, 0, 1/2), (1/3, 2/3, 1/6), (2/3, 1/3, 5/6)

6c: (0, 0, ±z), (1/3, 2/3, 2/3±z), (2/3, 1/3, 1/3±z)

Table S6. Refined parameters of pristine LiNiO₂.

LiNiO ₂						
	x	y	z	Wycoff site	Occupancy	U _{iso}
Li	0.000	0.000	0.000	3a	0.964	0.07034
Ni	0.000	0.000	0.000	3a	0.036	0.07034
Li	0.000	0.000	0.500	3b	0.036	0.04030
Ni	0.000	0.000	0.500	3b	0.964	0.04030
O	0.000	0.000	0.242	6c	1	0.05273

R_{wp} = 7.4%; R_p = 5.32%; cation mixing = 3.6%**Table S7.** Refined parameters of 2% Ga doped LiNiO₂.

2% Ga doped LiNiO ₂						
	x	y	z	Wycoff site	Occupancy	U _{iso}
Li	0.000	0.000	0.000	3a	0.983	0.00997
Ga	0.000	0.000	0.000	3a	0.017	0.00997
Ga	0.000	0.000	0.500	3b	0.001	0.01505
Ni	0.000	0.000	0.500	3b	0.999	0.01505
O	0.000	0.000	0.239	6c	1	0.01771

R_{wp} = 7.12%; R_p = 5.57%**Table S8.** Refined parameters of 5% Ga doped LiNiO₂.

5% Ga doped LiNiO ₂						
Phase 1: Ga-doped LiNiO ₂						
	x	y	z	Wycoff site	Occupancy	U _{iso}
Li	0.000	0.000	0.000	3a	0.984	0.03070
Ga	0.000	0.000	0.000	3a	0.016	0.03070
Ga	0.000	0.000	0.500	3b	0.004	0.03985
Ni	0.000	0.000	0.500	3b	0.989	0.03985
O	0.000	0.000	0.239	6c	1	0.04885
Phase 2: LiGaO ₂						
Ga	0.000	0.000	0.500	3b	1	0.01689
Li	0.000	0.000	0.000	3a	1	0.04909
O	0.000	0.000	0.241	6c	1	0.21350

R_{wp} = 8.47%; R_p = 5.86%

EDS line scan simulation assuming a core-shell particle configuration

The pseudocode for computing signal expectation based on a core-shell particle model is shown below. The beam penetration at position x in the Ga-rich and Ni-rich domains is a proxy for the signal strength from each element.

Function EDS_signal_estimate(R_o , R_i , NominalPenetration, x):

```

# x is referenced from the particle center (0, 0)
if  $R_o < R_i$ : raise Exception

OuterSliceDepth =  $2 * (R_o^2 - x^2)^{1/2}$  if ( $R_o > |x|$ ) else 0
InnerSliceDepth =  $2 * (R_i^2 - x^2)^{1/2}$  if ( $R_i > |x|$ ) else 0
ProbeLength = min( NominalPenetration, OuterSliceDepth )
ShellLength = (OuterSliceDepth - InnerSliceDepth)/2
SurfaceToFarCoreLength = ShellLength + InnerSliceDepth
# Signals calculation
if InnerSliceDepth != 0:
    if Probe Length < SurfaceToFarCoreLength:
        Ga = min(ProbeLength,ShellLength)
        Ni = max[(ProbeLength - Ga),0]
    else:
        Ga = ProbeLength - InnerSliceDepth
        Ni = ProbeLength - Ga
else:
    Ga = ProbeLength
    Ni = 0

```

Return (Ga, Ni)

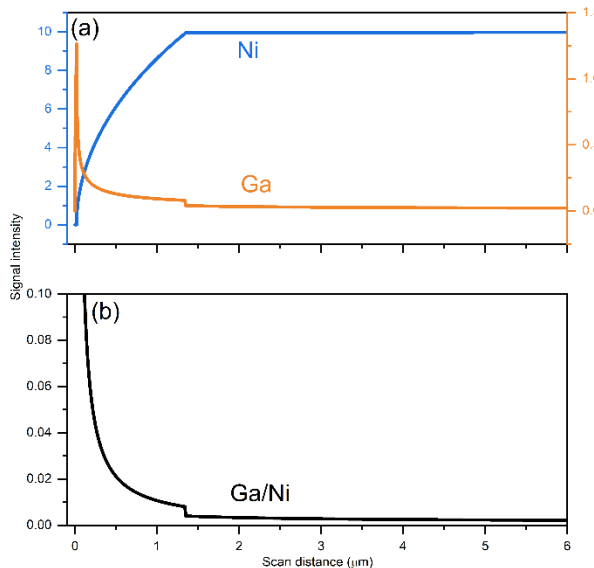


Fig. S5. Simulation of EDS line scan signal intensity versus scan distance from the particle edge inward assuming a spherical particle: 20 μm particle outer diameter, 20 nm Ga shell, and a constant beam penetration depth of 10 μm . A Ga-rich shell and Ni-rich core are assumed for the simulation. Simulation data is presented over 6 μm starting from the particle left edge.

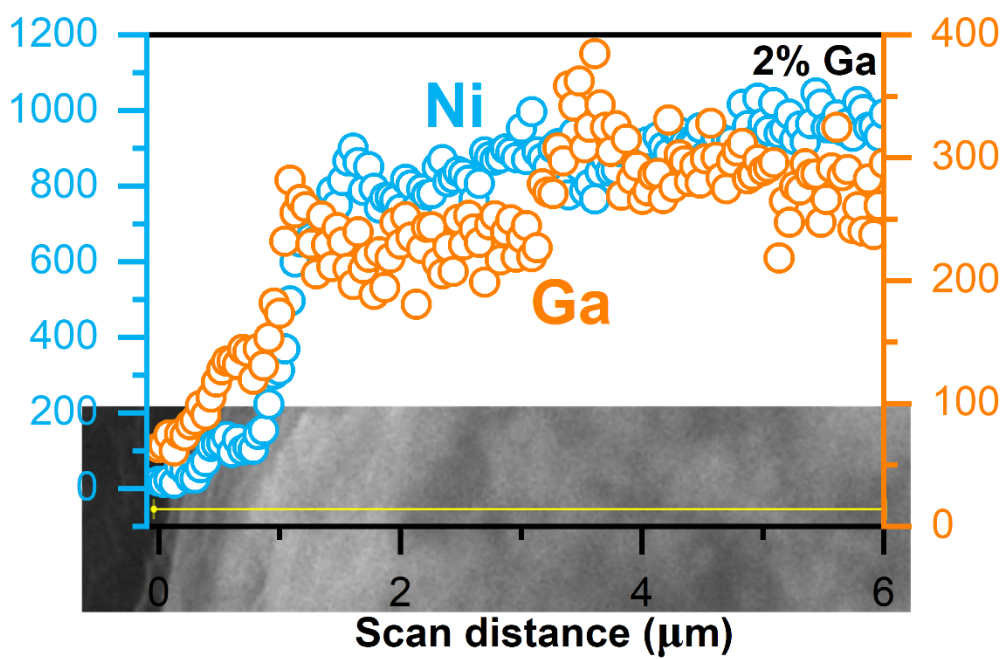


Fig. S6. Line scan EDS profile of 2% Ga-LiNiO₂. The image inset between is the actual SEM image during the line scan.

Estimation of theoretical specific capacities

Table S9. Capacity calculation for 0%, 2%, and 5% Ga-LiNiO₂ electrodes.

Electrodes	Theoretical capacity (mAh·g ⁻¹)	Experimental initial charge capacity (mAh·g ⁻¹) (at 0.1C)
0% Ga-LiNiO ₂	274.52 (1mol Li)	221.56 (0.81 mole Li)
2% Ga-LiNiO ₂	273.90 (1 mol Li)	213.33 (0.79 mole Li)
5% Ga-LiNiO ₂	268.16 (1 mole Li)	203.85 (0.77 mole Li)

Electrochemical impedance spectroscopy (EIS) of electrodes in half-cells before and after cycling

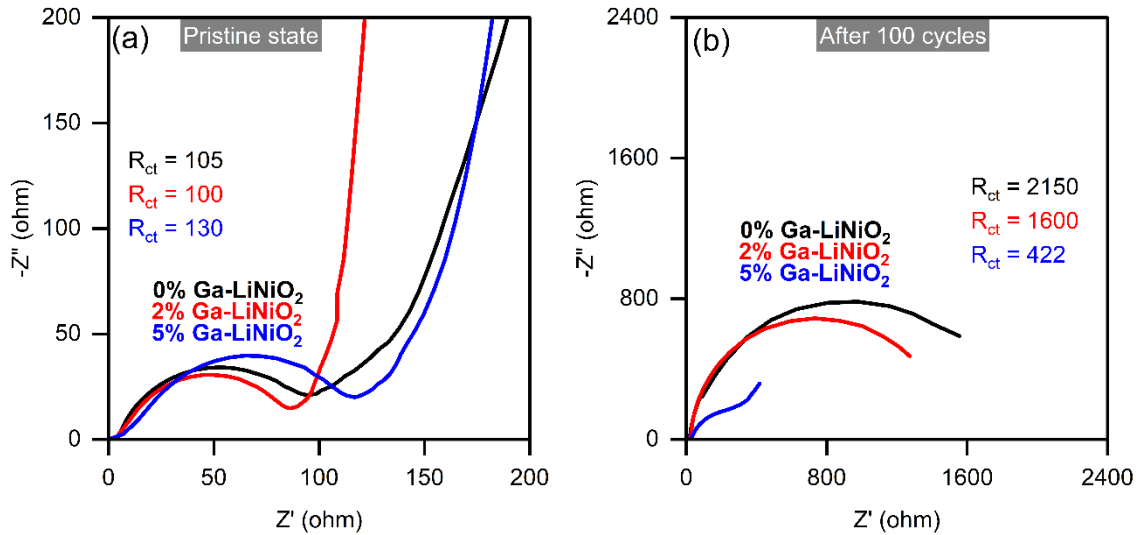


Fig. S7. EIS Nyquist plot of (a) as-assembled and (b) cycled 0%, 2%, and 5% Ga-LiNiO₂ half-cells. The estimated charge transfer resistances R_{ct} are shown in the figures.

The impedance spectra (EIS) of as-assembled half-cells reveal a slightly higher charge transfer resistance (R_{ct}) in the 5% Ga-doped cathode (**Fig. S7a**) attributable to the presence of surface α -LiGaO₂. However, after 100 cycles, the R_{ct} for the 0% (~ 2150 Ω) and solution-doped 2% (~ 1600 Ω) Ga-LiNiO₂ cells increased drastically compared to their 5% Ga-doped counterpart (**Fig. S7b**). This increased resistance is likely from surface reconstruction and the particle pulverization providing higher surface area for excessive growth of resistive cathode-electrolyte interphases (CEI). Conversely, the increase in R_{ct} for 5% Ga-LiNiO₂ at cycle 100 is markedly lower (~ 422 Ω), underscoring the protective effect of the LiGaO₂ coating in mitigating surface degradation and particle breakage responsible for growing impedance.

Differential capacity analysis (dQ/dV) at C/10

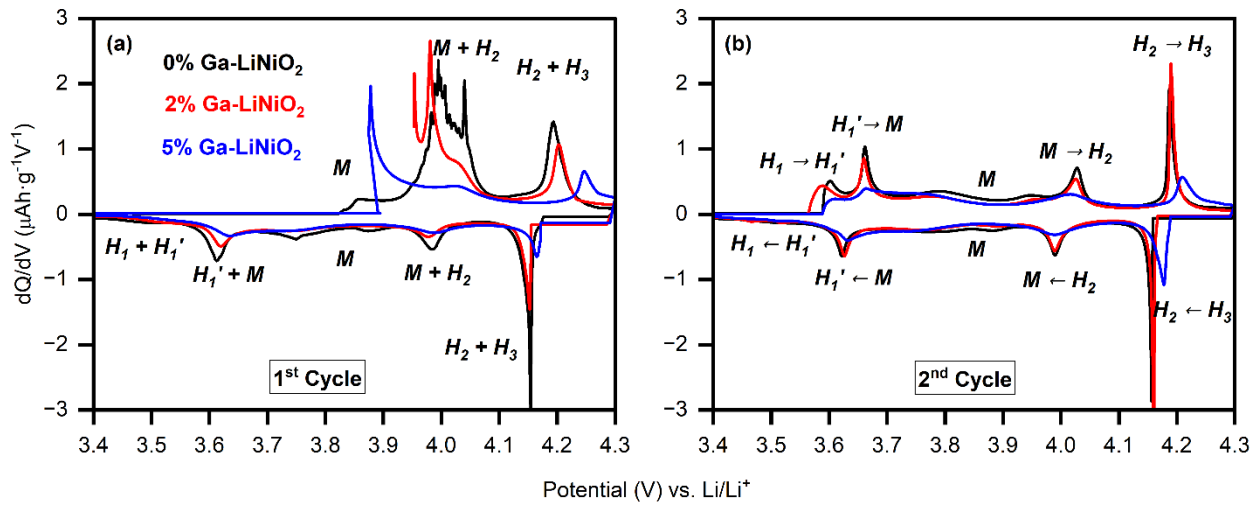


Fig. S8. dQ/dV at C/10 on the 1st (a) and 2nd (b) cycles of 0%, 2%, and 5% Ga-LiNiO₂.

Coulombic Efficiency (CE) profile

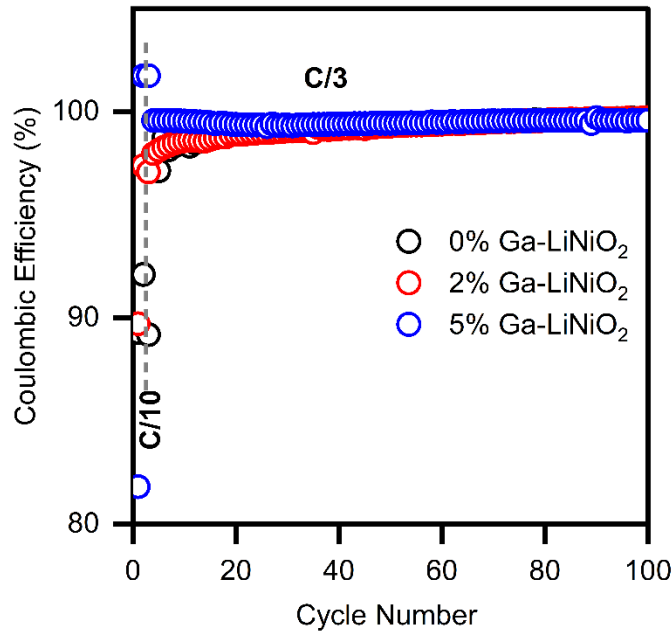


Fig. S9. Coulombic Efficiency profile of 0%, 2%, and 5% Ga-LiNiO₂.

Scanning electron microscopy (SEM) imaging of electrodes post 100 cycles

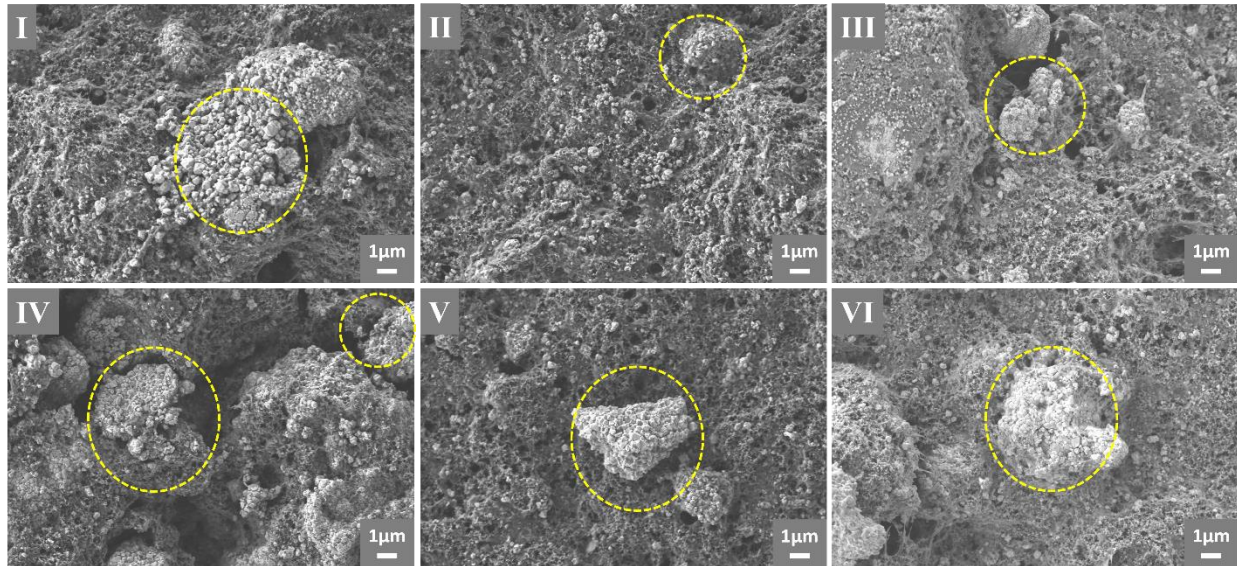


Fig. S10. SEM images of 0% Ga-LiNiO₂ electrodes obtained after 100 cycles at different locations showing numerous secondary particles are pulverized to primary nanoparticles.

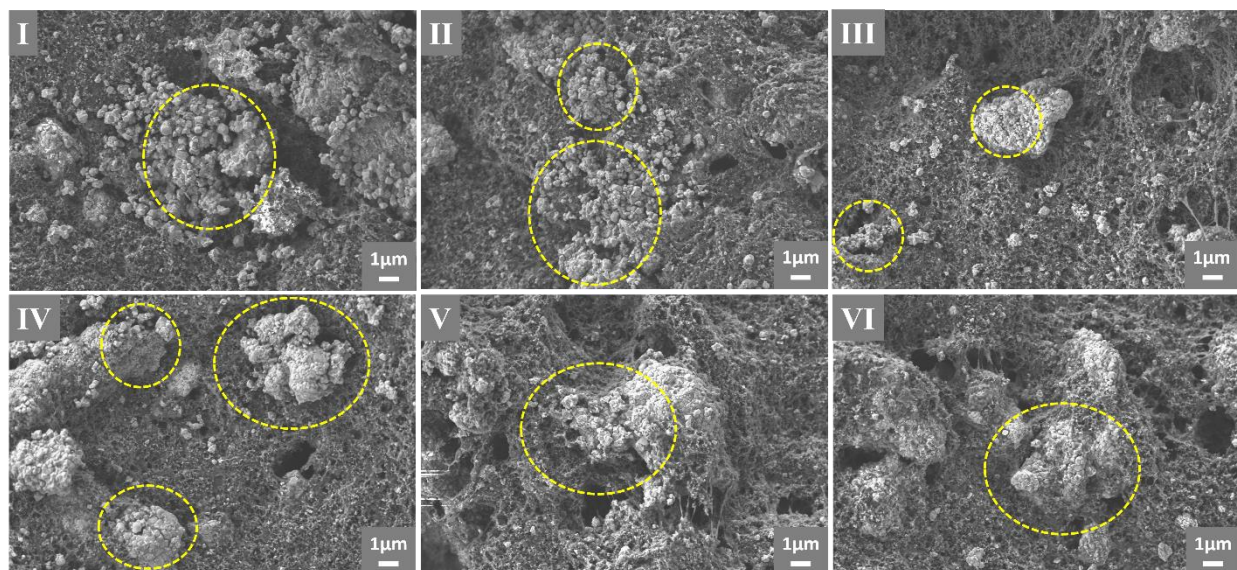


Fig. S11. SEM images of 2% Ga-LiNiO₂ electrodes obtained after 100 cycles at different locations also showing numerous secondary particles are pulverized to primary nanoparticles.

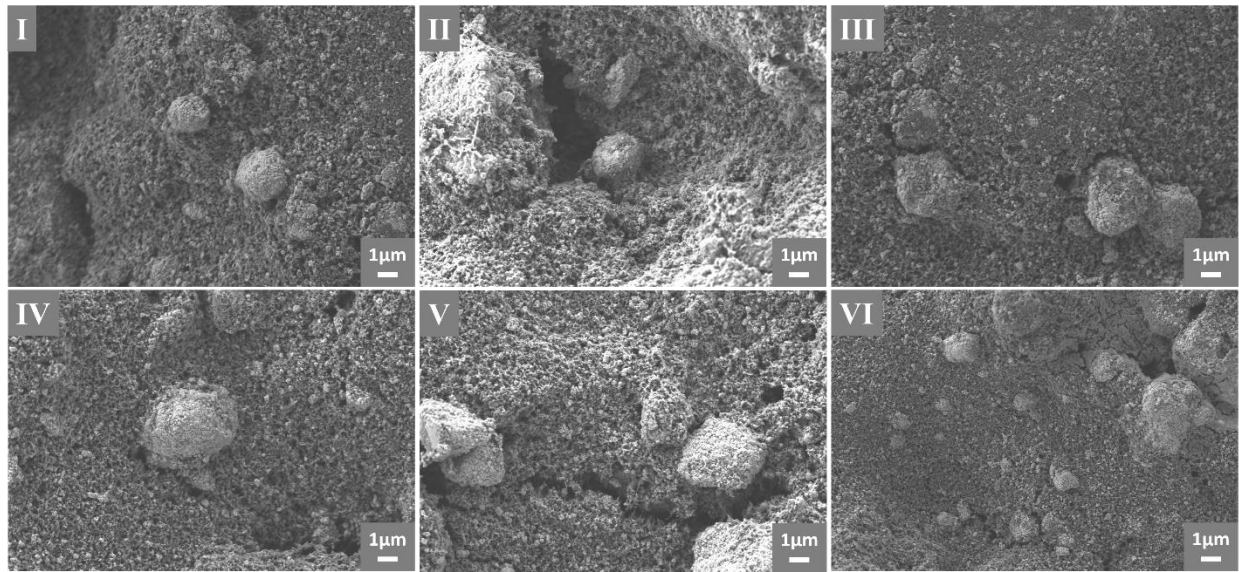


Fig. S12. SEM images of 5% Ga-LiNiO₂ electrodes obtained after 100 cycles at different locations showing minimal pulverization of secondary particles.

HRTEM image of 5% Ga-LiNiO₂ electrodes after 100 cycles

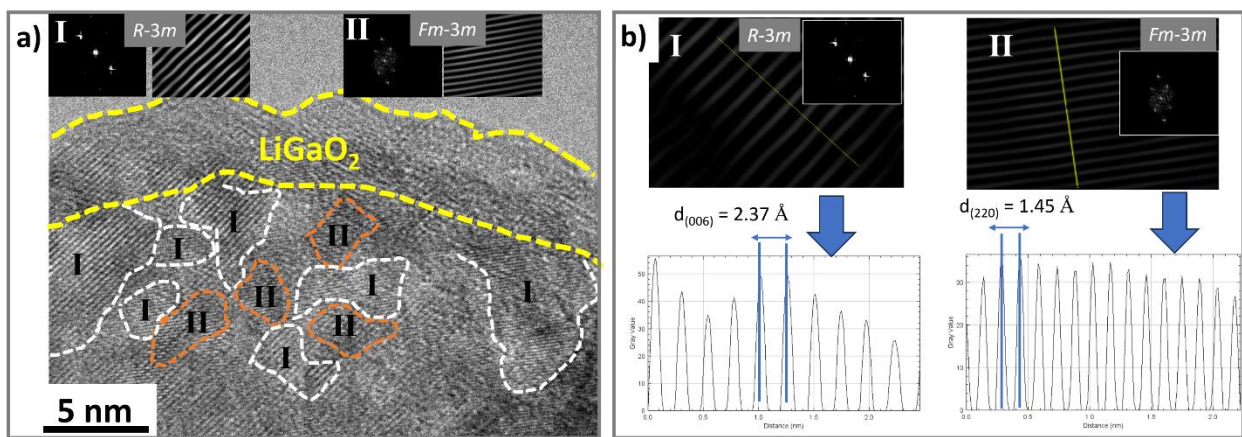


Fig. S13. a) HRTEM of 5% Ga-LiNiO₂ obtained after 100 cycles demonstrating $R\bar{3}m$ and $Fm\bar{3}m$ distribution at nanoscale near the surface. Region I correspond to $R\bar{3}m$ symmetry whereas Region II is the $Fm\bar{3}m$ rock-salt phase from reconstruction. b) d-spacing calculations of region I and II. FFT and corresponding IFFT images of one of the spots are shown inset for clarity.

REFERENCES

- 1 H. H. Ryu, G. T. Park, C. S. Yoon and Y. K. Sun, *J. Mater. Chem. A*, 2019, **7**, 18580–18588.
- 2 X.-Z. Kong, D.-L. Li, K. Lahtinen, T. Kallio and X.-Q. Ren, *J. Electrochem. Soc.*, 2020, **167**, 140545.
- 3 C. S. Yoon, U. H. Kim, G. T. Park, S. J. Kim, K. H. Kim, J. Kim and Y. K. Sun, *ACS Energy Lett.*, 2018, **3**, 1634–1639.
- 4 J. Li, Y. Zhu, B. Pang and P. Gao, *J. Mater. Sci.*, 2022, **57**, 17722–17734.
- 5 C. S. Yoon, M. J. Choi, D. W. Jun, Q. Zhang, P. Kaghazchi, K. H. Kim and Y. K. Sun, *Chem. Mater.*, 2018, **30**, 1808–1814.
- 6 W. M. Seong and A. Manthiram, *ACS Appl. Mater. Interfaces*, 2020, **12**, 43653–43664.
- 7 G.-X. Huang, R.-H. Wang, X.-Y. Lv, J. Su, Y.-F. Long, Z.-Z. Qin and Y.-X. Wen, *J. Electrochem. Soc.*, 2022, **169**, 040533.
- 8 H. R. Park, *Journal of Industrial and Engineering Chemistry*, 2010, **16**, 698–702.
- 9 J. Cho, T. J. Kim, Y. J. Kim and B. Park, *Electrochem. Solid-State Lett.*, 2001, **4**, A159.
- 10 Y. Li, S. Deng, Y. Chen, J. Gao, J. Zhu, L. Xue, T. Lei, G. Cao, J. Guo and S. Wang, *Electrochim. Acta*, 2019, **300**, 26–35.
- 11 Y. Nishida, K. Nakane and T. Satoh, *J. Power Sources*, 1997, **68**, 561-564.
- 12 D. Kitsche, S. Schweidler, A. Mazilkin, H. Geßwein, F. Fauth, E. Suard, P. Hartmann, T. Brezesinski, J. Janek and M. Bianchini, *Mater. Adv.*, 2020, **1**, 639–647.
- 13 X. Kong, D. Li, E. O. Fedorovskaya, T. Kallio and X. Ren, *Int. J. Energy Res.* 2021, **45**, 10489–10499.
- 14 K. Y. Park, Y. Zhu, C. G. Torres-Castanedo, H. J. Jung, N. S. Luu, O. Kahvecioglu, Y. Yoo, J. W. T. Seo, J. R. Downing, H. D. Lim, M. J. Bedzyk, C. Wolverton and M. C. Hersam, *Adv. Mater.* 2022, **34**, 2106402.
- 15 H. Cao, F. Du, J. Adkins, Q. Zhou, H. Dai, P. Sun, D. Hu and J. Zheng, *Ceram. Int.*, 2020, **46**, 20050–20060.
- 16 S. H. Park, K. S. Park, Y. Kook Sun, K. S. Nahm, Y. S. Lee and M. Yoshio, *Electrochim. Acta*, 2001, **46**, 1215-1222.
- 17 Yang G, Qin X, Wang B, Cai F, Gao J. *Journal of Materials Research*. 2020; **35**(1): 51-57.
- 18 T. Kim, L. K. Ono, Y. Qi, *J. Mater. Chem. A*, 2023, **11**, 221-231.
- 19 L. Wu, X. Tang, X. Chen, Z. Rong, W. Dang, Y. Wang, X. Li, L. Huang, Y. Zhang, *j. Power Sources*, 2020, **445**, 227337.
- 20 J. T. Wolan and G. B. Hoflund, *J. Vac. Sci. Technol. A*, 1998, **16**, 3414.
- 21 <https://www.thermofisher.com/us/en/home/materials-science/learning-center/periodic-table/other-metal/gallium.html>.

Supplementary XRD refinement information clipped from the GSAS-II software. The tables below show improper refinement convergence under various conditions considered. These analyses exclude certain occupancy possibilities.

(a) Refining site occupancy and Uiso value of 2% Ga-LiNiO₂ when assuming Ga occupies only 3a site.

	Name	Type	refine	x	y	z	frac	site sym	mult	I/A	Uiso
0	Ni2	Ni+3	FU	0.00000	0.00000	0.50000	1.0119	-3m(100)	3	I	0.02267
1	Ga2	Ga+3	FU	0.00000	0.00000	0.00000	-0.0228	-3m(100)	3	I	-0.01034
2	Li2	Li+1	FU	0.00000	0.00000	0.00000	1.3487	-3m(100)	3	I	-0.01034
3	O1	O-2		0.00000	0.00000	0.23924	1.0000	3m(100)	6	I	0.02418

	Name	Type	refine	x	y	z	frac	site sym	mult	I/A	Uiso
0	Ni1	Ni+3	FU	0.00000	0.00000	0.50000	0.5824	-3m(100)	3	I	0.07930
1	Ga1	Ga+3	FU	0.00000	0.00000	0.00000	-0.1995	-3m(100)	3	I	0.09034
2	Li1	Li+1	FU	0.00000	0.00000	0.00000	1.1995	-3m(100)	3	I	0.09034
3	O1	O-2	XU	0.00000	0.00000	0.24329	1.0000	3m(100)	6	I	0.00343

(b) Refining site occupancy and Uiso value of 2% Ga-LiNiO₂ when assuming Ga occupies only 3b site.

	Name	Type	refine	x	y	z	frac	site sym	mult	I/A	Uiso
0	Ni1	Ni+3	U	0.00000	0.00000	0.50000	0.9800	-3m(100)	3	I	0.48393
1	Ga1	Ga+3	U	0.00000	0.00000	0.50000	0.0200	-3m(100)	3	I	0.51607
2	Li1	Li+1	U	0.00000	0.00000	0.00000	1.0000	-3m(100)	3	I	-2.89599
3	O1	O-2		0.00000	0.00000	0.23924	1.0000	3m(100)	6	I	0.02418

	Name	Type	refine	x	y	z	frac	site sym	mult	I/A	Uiso
0	Ni1	Ni+3	FU	0.00000	0.00000	0.50000	0.9524	-3m(100)	3	I	0.02330
1	Ga1	Ga+3	FU	0.00000	0.00000	0.50000	0.0476	-3m(100)	3	I	0.02330
2	Li1	Li+1	FU	0.00000	0.00000	0.00000	1.0460	-3m(100)	3	I	-3.66347
3	O1	O-2		0.00000	0.00000	0.23924	1.0000	3m(100)	6	I	0.02418